

Crystal chemistry of NaMgF₃ perovskite at high pressure and temperature

JIUHUA CHEN,* HAOZHE LIU,† C. DAVID MARTIN, JOHN B. PARISE, AND DONALD J. WEIDNER

Mineral Physics Institute, State University of New York at Stony Brook, Stony Brook, New York 11794-2100, U.S.A.

ABSTRACT

The crystal structure of NaMgF₃ perovskite (neighborite) has been studied at 4 GPa and temperatures up to 1000 °C using the Rietveld structure-refinement method. In situ synchrotron X-ray powder diffraction data was collected using monochromatic radiation. The orthorhombic (*Pbnm*) to cubic (*Pm $\bar{3}$ m*) transition was observed when the temperature increased from 900 to 1000 °C. Structure refinements show that the ratio of polyhedral volumes of the A and B sites (V_A/V_B) of the orthorhombic phase increases with temperature, approaching the ideal value (5) for the cubic structure. However, this ratio becomes smaller at 4 GPa compared to the result from previous studies at the same temperature but ambient pressure, indicating that pressure makes it more difficult to transform from the orthorhombic phase to the cubic phase in this kind of perovskite.

INTRODUCTION

Geophysical interest in the perovskite family of materials dates from Ringwood's proposing that Earth's lower mantle is dominated by iron-bearing MgSiO₃ perovskite (Ringwood 1962). Until now, however, knowledge about the crystal chemistry of this mineral at lower mantle pressure and temperature conditions is very limited. MgSiO₃ perovskite is stable only at pressures beyond about 23 GPa (Ito and Yamada 1982), and high quality diffraction data are very difficult to obtain at such high pressures due to several limitations on experimental techniques. Several provocative proposals of decomposition and phase transitions in Ca- and MgSiO₃-related materials have far-reaching implications for the composition and structure of the lower mantle (Saxena et al. 1996, 1998; Shim et al. 2001, 2002). Although a transmission electron microscopy (TEM) study showed a hint of an orthorhombic-cubic phase transition in the iron-bearing MgSiO₃ perovskite system (Wang et al. 1992), more detailed investigations on the effect of pressure, temperature, and composition on lattice parameters and the density of iron-bearing MgSiO₃ perovskite indicated a trend of more structural distortion with increasing pressure (Mao et al. 1991). A recent study indicates that MgSiO₃ perovskite transforms to a new high-pressure phase at 125 GPa (Murakami et al. 2004). This pressure corresponds to the depth near the base of the mantle. Therefore the perovskite phase still dominates the Earth's lower mantle. A fundamental understanding of the behavior of selected representatives of the perovskite family of structures to high-pressure/high-temperature conditions is valuable for establishing possible behaviors for this family in general. We have chosen to study NaMgF₃ perovskite (neighborite) and its solid solution with KMgF₃ as it has gained significant attention as an analogue material of MgSiO₃ perovskite (Chakhmouradian et al. 2001; O'Keefe and Bovin 1979; O'Keefe et al. 1979; Rönnebro et al. 2000; Street

et al. 1997; Zhao et al. 1994a, 1994b, 1993a, 1993b; Zhou et al. 1997). Neighborite is isoelectronic with MgSiO₃, and they are isostructural, possessing the same type of distortion from the ideal cubic perovskite structure to crystallize in space group *Pbnm*.

NaMgF₃ perovskite was first synthesized (Ludekens and Welch 1952) before natural NaMgF₃ was discovered (Chao et al. 1961). The mineral was initially found in an oil shale of the Utah Green River formation (named neighborite after geologist Frank Neighbor), and was crystallographically described by Chao et al. (1961). Although O'Keefe et al. (O'Keefe and Bovin 1979; O'Keefe et al. 1979) pointed out the structural similarity between NaMgF₃ and MgSiO₃ in the late 1970s, systematic studies of the NaMgF₃ structure did not start until a decade ago. Following an extensive study of the NaMgF₃ structure and its temperature-induced phase transition by Zhao et al. (Zhao et al. 1994a, 1994b, 1993a, 1993b), several experimental and theoretical studies have been reported (Chakhmouradian et al. 2001; Rönnebro et al. 2000; Street et al. 1997; Zhou et al. 1997). Using the "macroscopic" relation between the structural distortion and unit-cell dimensions described by O'Keefe and Hyde (1977), Zhao et al. (1994b) investigated the pressure and temperature dependence of the structural distortion, and demonstrated two decoupled mechanisms for thermal expansion and compression, i.e., thermal expansion is mostly accommodated by octahedral tilting and compression is dominated by changes in the octahedral bond lengths. However, no structure refinement had been done for a sample maintained simultaneously at high pressure and temperature to study the pressure effect on the structure distortion from a microstructure point of view. Derivation of the microscopic atomic parameters from cell parameters alone, as was proposed by O'Keefe and Hyde (1977) and Zhao et al. (1994b), is only accurate when the assumption of rigid octahedra is valid. This does not appear to be the case at high pressure (Zhao et al. 1994a). In this paper, we present crystal chemistry data derived from structure refinements based on X-ray diffraction data collected at high pressure and high temperature.

* E-mail: Jiuhoa.Chen@sunysb.edu

† Present address: HPCAT, Advanced Photon Source, Argonne National Laboratory, Argonne, Illinois 60439-4803, U.S.A.

EXPERIMENTAL METHOD

The synthetic sample used in the present study was synthesized by Zhao and the synthesis procedure can be found in Zhao et al. (1993a). This sample was identical to that used in the previous studies by Zhao et al. (Zhao et al. 1994a, 1994b, 1993a, 1993b). In situ monochromatic X-ray diffraction data was obtained at the superconductor wiggler beam line, X17B, of the National Synchrotron Light Source (NSLS). Pressure was generated by using DIA-type cubic anvil press SAM85 (Weidner et al. 1992). A sketch of the high-pressure cell assembly is shown in Figure 1. Disc heaters were used in the cell assembly to minimize the number of materials in the X-ray path. A layer of NaCl powder was placed next to the sample as an internal pressure calibrant. The pressure was calculated based on Decker's equation of state of NaCl (Decker 1971). The temperature was measured using a W3%Re-W25%Re thermocouple placed between the sample and the NaCl powder. The pressure medium was made of a mixture of amorphous boron and epoxy resin (4:1). The finely powdered sample and the NaCl powder were loaded in a pressure-medium sleeve 1 mm in diameter. Each layer of sample and NaCl was about 0.5 mm thick.

A translating image plate system (Chen et al. 1998b) was used to collect powder X-ray diffraction patterns. The incident beam has a cross section size of 0.2×0.2 mm and an energy of 40.61(1) keV [or 0.3053(1) Å, calibrated using a germanium solid-state detector]. There was no collimation for the diffracted X-rays. Parasitic scattering contributing to the diffraction patterns, from the boron-epoxy pressure transmitting medium, were subtracted using the data collected from the pressure medium alone at the same *P/T* conditions as the sample plus medium. Details about the background subtraction are described elsewhere (Chen et al. 1998a). The imaging plate detector was placed about 800 mm downstream from the press. An accurate sample-to-detector distance was calibrated using the radii of Debye-Scherrer rings from the same diffraction line recorded on two fix-distanced imaging plates.

Following compression at ambient temperature, the sample was heated to 600 °C to anneal out the internal stress induced by grain-to-grain contact during compression. Previous studies have demonstrated that this temperature is efficient to completely release the sample stress and does not cause significant grain growth. After the annealing we obtained sharp and smooth diffraction lines on the image plate confirming the quality of the sample. The sample temperature was then increased step wise up to 1000 °C. Diffraction patterns were collected at 25, 200, 400, 600, 700, 800, 900, and 1000 °C. A significant drop in cell pressure was observed during the annealing heating cycle. The pressure during the data collection was maintained at 4 ± 0.5 GPa. No evidence of reactions between the sample and surrounding materials could be observed in the X-ray diffraction patterns. The Rietveld refinements were performed with GSAS, the General Structure Analysis System (Larson and Von Dreele 1986). An example of refined diffraction patterns is shown in Figure 2.

RESULT AND DISCUSSIONS

At 4 GPa NaMgF₃ perovskite transforms from orthorhombic to cubic symmetry between the temperatures of 900 and 1000 °C

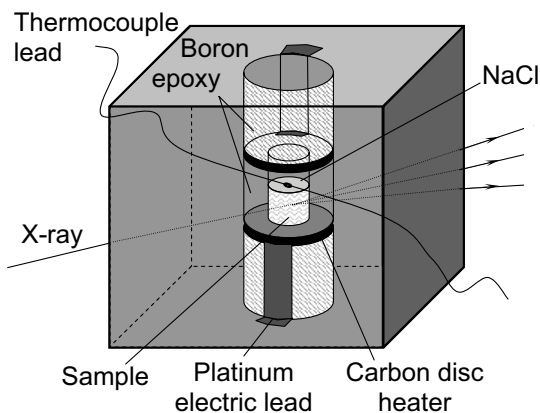


FIGURE 1. Cubic high pressure cell assembly for monochromatic X-ray diffraction experiments.

(Fig. 2). The structural parameters refined at all 8 temperatures are listed in Table 1. Variations of the unit-cell dimensions and volume with temperature are illustrated in Figure 3, after converting the orthorhombic unit cell ($a, b, c; Z = 4$) to a reduced pseudo-cubic cell ($a_p = a/\sqrt{2}, b_p = b/\sqrt{2}, c_p = c/2, Z = 1$, Fig. 4). With increasing temperature the cell dimension (a_p, b_p, c_p) continuously converge toward a cubic cell consistent with the temperature dependence of the cell dimension observed at ambient pressure (Zhao et al. 1993a). Although the cell dimension apparently becomes metrically tetragonal cell ($b_p \approx c_p$) at 900 °C, before the orthorhombic to cubic phase transition, neither a disappearance of (120, 210) and (122, 212) diffraction peaks of the orthorhombic phase (due to possible $I4/mcm$ tetragonal symmetry) nor the vanishing of (121, 103, 211) diffraction peaks (due to possible $P4/mbm$ tetragonal symmetry) was observed. This indicates that the true symmetry of the lattice at 900 °C

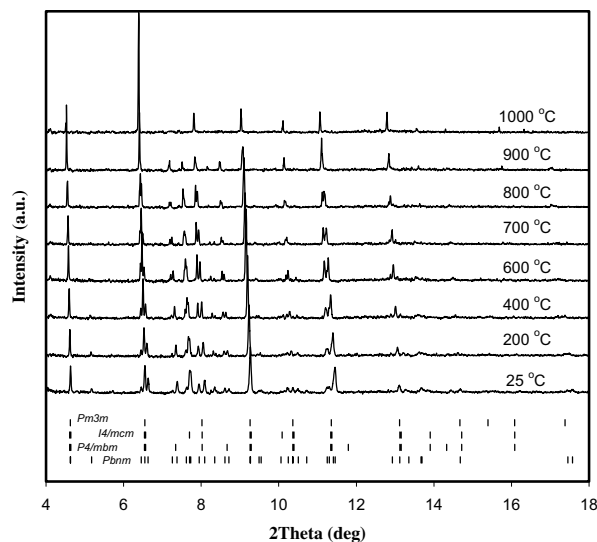


FIGURE 2. X-ray diffraction patterns of NaMgF₃ collected using imaging plate and a monochromatic beam ($E = 40.61$ keV) at 4 GPa.

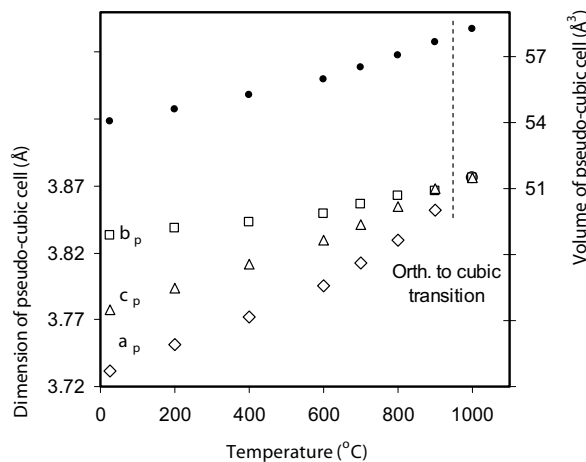


FIGURE 3. Temperature dependence of the pseudo-cubic cell ($a_p = a/\sqrt{2}, b_p = b/\sqrt{2}, c_p = c/2, V_p = V/4, Z = 1$) of NaMgF₃ at 4 GPa. Experimental uncertainties of the data are less than the size of the symbols.

TABLE 1. Structural parameters of NaMgF₃ at 4 GPa

<i>T</i> (°C)	25	200	400	600	700	800	900	1000
Space group				<i>Pbnm</i>				<i>Pm3m</i>
<i>a</i>	5.2768(3)	5.3047(4)	5.3350(2)	5.3678(2)	5.3915(3)	5.4162(3)	5.4480(9)	3.8760(1)
<i>b</i>	5.4213(6)	5.4282(6)	5.4352(4)	5.4440(3)	5.4532(3)	5.4629(3)	5.4677(9)	3.8760(1)
<i>c</i>	7.5548(6)	7.5864(7)	7.6227(5)	7.6587(3)	7.6831(4)	7.7092(5)	7.7366(5)	3.8760(1)
Na <i>x</i>	0.9877(5)	0.9856(8)	0.9893(8)	0.9930(8)	0.9988(7)	0.9980(9)	0.9967(9)	0
<i>y</i>	0.0493(4)	0.0455(6)	0.0377(5)	0.0296(9)	0.0286(9)	0.0242(9)	0.0191(9)	0
<i>z</i>	0.25	0.25	0.25	0.25	0.25	0.25	0.25	0
<i>U</i> (Å ³)	0.035(2)	0.036(2)	0.038(2)	0.051(2)	0.053(2)	0.064(3)	0.121(4)	0.111(5)
Mg <i>x</i>	0	0	0	0	0	0	0	0.5
<i>y</i>	0.5	0.5	0.5	0.5	0.5	0.5	0.5	0.5
<i>z</i>	0	0	0	0	0	0	0	0.5
<i>U</i> (Å ³)	0.015(1)	0.014(2)	0.012(1)	0.021(1)	0.018(2)	0.025(2)	0.053(2)	0.046(3)
F(1) <i>x</i>	0.0892(9)	0.0870(9)	0.0812(4)	0.0788(8)	0.0697(17)	0.0607(22)	0.0307(66)	0.5
<i>y</i>	0.4677(9)	0.4669(9)	0.4732(9)	0.4783(9)	0.4842(19)	0.4914(31)	0.4788(72)	0.5
<i>z</i>	0.25	0.25	0.25	0.25	0.25	0.25	0.25	0
<i>U</i> (Å ³)	0.027(3)	0.018(4)	0.024(3)	0.036(3)	0.034(3)	0.058(5)	0.580(36)	0.135(4)
F(2) <i>x</i>	0.6963(8)	0.6951(6)	0.7000(9)	0.7017(9)	0.7078(11)	0.7028(13)	0.7240(18)	–
<i>y</i>	0.2968(9)	0.2956(7)	0.2952(9)	0.2970(9)	0.2978(12)	0.2884(12)	0.2835(16)	–
<i>z</i>	0.0546(9)	0.0481(9)	0.0461(9)	0.0408(8)	0.0396(11)	0.0407(13)	0.0295(18)	–
<i>U</i> (Å ³)	0.029(2)	0.033(3)	0.023(2)	0.035(2)	0.044(3)	0.048(3)	0.077(3)	–
<i>R</i> _p	0.132	0.152	0.131	0.121	0.138	0.144	0.170	0.167
<i>R</i> _{wp}	0.180	0.226	0.171	0.169	0.192	0.197	0.228	0.215
χ ²	9.70	12.87	9.04	9.12	9.08	9.90	12.2	12.86

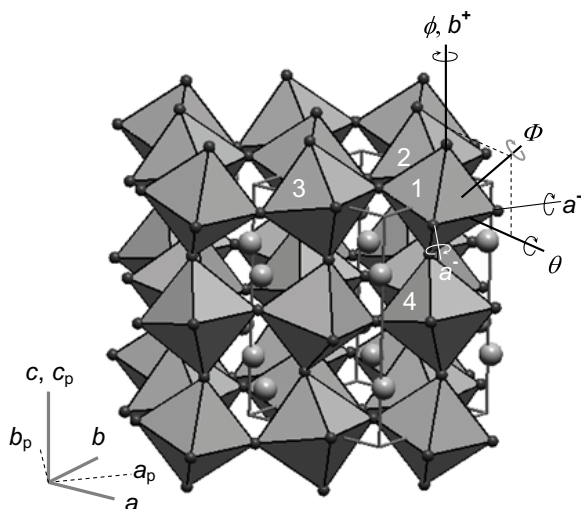


FIGURE 4. Crystal structure of NaMgF₃ at 700 °C and 4 GPa. Dark and grey spheres represent F and Na, respectively. Octahedra represent the MgF₆ sites. The unit cell (*Pbnm*) and *a*, *b*, *c* distances are shown in the structure. *a_p*, *b_p*, *c_p* represent the dimensions of the pseudo-cubic cell (*a_p* = *a*/√2, *b_p* = *b*/√2, *c_p* = *c*/2, *Z* = 1). (*a_p*, *b_p*, *c_p*) axes: any consecutive two octahedra (e.g., 1 and 3) about (100)_p axis tilt in opposite direction; any consecutive two octahedra (e.g., 1 and 2) about (010)_p axis also tilt in the opposite direction, and the magnitude of tilting about (100)_p and (010)_p are the same; and any two consecutive octahedra (e.g., 1 and 4) about (001)_p axis tilt in the same direction. ϕ and θ indicate the two independent tilting angles about (001)_p and (110)_p, which define a compound angle Φ about the “threefold axes” (111)_p.

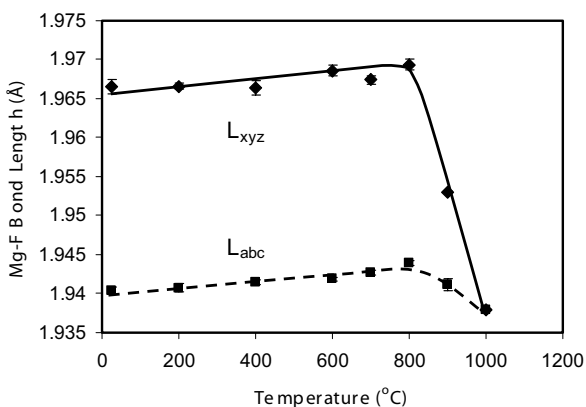
remains orthorhombic. On the other hand, we noticed that when the temperature approached the transition temperature intensities of the (121, 103, 211) peaks decreased more rapidly than those of the (120, 210) and (122, 212) peaks (Fig. 2). Zhao et al. (1993b)

also observed a faster decrease of (121, 103, 211) peak intensities near the orthorhombic-cubic transition temperature at ambient pressure, but the dimensions of the reduced pseudo-cubic cell never become tetragonal before the phase transformation at ambient pressure. Therefore, pressure seems to enhance the possibility of the existence of a *P4/mbm* tetragonal intermediate phase between the orthorhombic and cubic phases. Although Zhao et al. (1993b) did not observe tetragonal cell dimensions for the pseudo-cubic cell near the transition temperature in their later in situ energy-dispersive X-ray diffraction experiments at high pressures, their highest-pressure data (9.5 GPa) shows a cross over of the values of *b_p* and *c_p* near the transition temperature, i.e., *c_p* becomes bigger than *b_p* at 1100 °C. The *P4/mbm* tetragonal structure has been found to be an intermediate phase between the orthorhombic and cubic phase in the K_xNa_{1-x}MgF₃ system as the composition (*x*) varies. The evolution of the cell dimensions from orthorhombic to tetragonal in our experiment (i.e., *b_p* = *c_p*) is different from that reported by Chao et al. (1961) (i.e., *a_p* = *b_p*), but consistent with that observed in the K_xNa_{1-x}MgF₃ system. Both the cell dimensions and the volume changes smoothly across the orthorhombic to cubic phase boundary, indicating a higher-order phase transition.

Selected Na-F and Mg-F interatomic distances and bond angles of MgF₆ octahedra were calculated from the atomic positions at different temperatures and listed in Table 2. Changes of mean (Mg-F) bond length as a function of temperature are plotted in Figure 5. Very similar to the situation observed at ambient pressure, when the temperature approaches the transition temperature the (Mg-F) bond length decreases with temperature. This phenomenon has been shown to be due to the large anisotropy in the distribution of F⁻ ions by a molecular-dynamics simulation (Street et al. 1997). Street et al. (1997) demonstrated that the maximum point of the Mg-F pair radial-distribution curve (detected by diffractions) shifts to shorter bond distances linearly

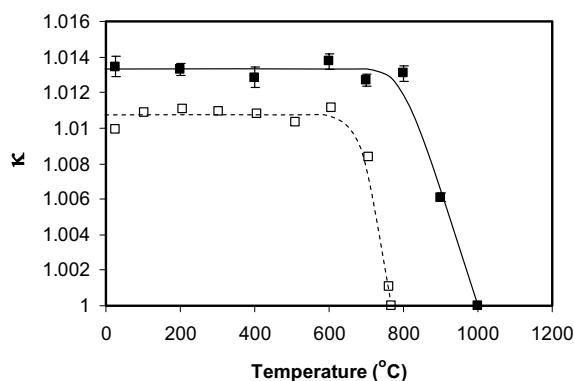
TABLE 2. Bond lengths and bond angles of NaMgF₃ determined at 4 GPa

<i>T</i> (°C)	25	200	400	600	700	800	900
Vector (Å)							
Na-F1	3.1982(1)	3.1865(9)	3.1071(7)	3.0364(8)	2.9932(9)	2.9304(3)	2.9600(9)
Na-F1	2.3306(7)	2.3498(4)	2.4173(1)	2.4858(3)	2.5137(3)	2.5748(1)	2.5203(8)
Na-F1	3.0762(5)	3.0673(1)	3.0637(6)	3.0820(5)	3.0746(9)	3.0313(3)	2.8817(9)
Na-F1	2.2760(4)	2.3070(1)	2.3180(4)	2.3154(3)	2.3390(3)	2.3969(9)	2.5841(3)
Na-F2 ×2	2.5187(1)	2.5620(2)	2.5994(5)	2.6704(5)	2.6888(9)	2.6913(5)	2.6846(2)
Na-F2 ×2	2.2351(1)	2.2594(1)	2.2744(5)	2.2941(5)	2.3319(6)	2.3336(8)	2.4526(4)
Na-F2 ×2	2.6839(6)	2.6634(6)	2.6801(4)	2.6658(9)	2.6677(4)	2.7020(2)	2.7156(9)
Na-F2 ×2	3.4054(7)	3.3781(5)	3.3340(6)	3.2874(2)	3.2590(5)	3.2503(1)	3.1191(2)
Mg-F1 ×2	1.9543(5)	1.9602(1)	1.9597(1)	1.9644(4)	1.9591(4)	1.9557(5)	1.9448(2)
Mg-F2 ×2	1.9879(9)	1.9950(4)	1.9809(9)	1.9705(6)	1.9469(2)	2.0064(5)	1.9273(2)
Mg-F2 ×2	1.9576(7)	1.9439(3)	1.9586(5)	1.9708(7)	1.9963(9)	1.9461(1)	1.9860(7)
Angle (°)							
F1-Mg-F1	180	180	180	180	180	180	180
F1-Mg-F2 ×2	86.788(2)	87.875(2)	87.956(2)	89.237(2)	88.687(2)	88.104(1)	84.993(5)
F1-Mg-F2 ×2	89.854(2)	91.111(2)	90.392(3)	90.750(3)	89.656(2)	87.446(2)	89.145(5)
F1-Mg-F2 ×2	93.212(2)	92.125(2)	92.044(2)	90.763(2)	91.313(2)	91.896(1)	95.007(5)
F1-Mg-F2 ×2	90.147(2)	88.889(2)	89.608(3)	89.250(2)	90.344(1)	92.554(1)	90.855(5)
F2-Mg-F2 ×2	89.152(7)	89.605(6)	89.332(5)	89.345(3)	89.013(4)	89.335(3)	89.220(9)
F2-Mg-F2 ×2	180	180	180	180	180	180	180
F2-Mg-F2 ×2	90.848(7)	90.395(6)	90.668(4)	90.655(3)	90.987(5)	90.665(3)	90.780(6)
Mg-F1-Mg	150.215(3)	150.731(3)	153.027(2)	154.163(4)	157.301(2)	160.446(2)	167.988(3)
Mg-F2-Mg	146.963(2)	148.907(2)	150.299(3)	151.809(2)	153.008(3)	153.384(2)	160.947(3)

**FIGURE 5.** Mean (Mg-F) bond length of NaMgF₃ at 4 GPa derived from atomic coordinates (L_{xyz}) and from the lattice parameters (L_{abc}). Bars attached to the symbols represent the experimental errors.

with increasing temperature while a long tail of the distribution curve extended to the larger bond-length side results in an increase of the bond distance with temperature. However, this interpretation does not illustrate why the apparent bond-length contraction is detected by diffractions only when the temperature is near the transition temperature. Phonon softening of anti-phase tilting and in-phase tilting as discussed by Zhao et al. (1993b) must play an important role in this bond-length anomaly. Clearly an investigation of this behavior using total scattering studies (Egami and Billinge 2003), where the constraints imposed by space group symmetry are lifted, would add much to our understanding of the underlying mechanism giving rise to the apparent Mg-F distance shortening.

Figure 5 also shows the (Mg-F) bond length derived from the lattice parameters (a , b , c) assuming undistorted MgF₆ octahedra in the structure. The ratio of the bond length (L_{xyz}) derived from the atomic coordinates (x , y , z) and the bond length (L_{abc}) derived from the lattice parameters (a , b , c), $\kappa = L_{xyz}/L_{abc}$, reflects the degree of the octahedra distortion in the real structure. The greater the value of κ the greater the distortion of the MgF₆ octahedra,

**FIGURE 6.** Ratio of the bond length (L_{xyz}) derived from atomic coordinates (x , y , z) to that (L_{abc}) derived from the lattice parameters (a , b , c) of NaMgF₃ at 4 GPa (solid symbols) and ambient pressure (open symbols, after Zhao et al. 1993a). Bars attached to the symbols represent the experimental errors.

with $\kappa=1$ for undistorted octahedra. Figure 6 shows the κ ratio at ambient pressure and high pressure, indicating that pressure enhances the octahedron distortion. When the temperature approaches the transition temperature, this distortion vanishes.

Another measure of the lattice distortion from the ideal cubic ($Pm\bar{3}m$) perovskite structure is octahedral tilting. As shown in Figure 4, the octahedral tilting in the perovskite structure can be described as ($a^-a^+c^+$) with Glazer notation (the letters specify the magnitude of the rotation about each axis of the three Cartesian axes). The superscripts +, -, and 0 indicate whether the rotations in adjacent layers are in the same or opposite direction, or if there is no rotation at all. The same structure was described as ($a^-b^+a^-$) by Glazer (1972) because of difference in the lattice axis selection. Zhao et al. (1993a) discussed that the three tilting angles can be converted into two independent tilts θ and ϕ (Fig. 4) in the orthorhombic perovskite structure with space group $Pbnm$. These two angles actually define a compound angle Φ about the “threefold axes” of the regular octahedron (Fig. 4). Table

3 lists all the tilting angles derived from our experimental data based upon the relations described by Zhao et al. (1993b). The tilting angles decrease with temperature, and approach zero as the temperature reaches the transition temperature. Comparison of these tilting angles with those obtained at ambient pressure (Fig. 7) demonstrates a pressure-enhanced octahedral tilting in the perovskite structure.

Alternatively, the degree of structure distortion can be evaluated using the volume ratio (V_A/V_B) between NaF₁₂ and MgF₆ polyhedra. Thomas (Thomas 1996, 1998) proposed a global parameterization method to quantitatively describe all perovskite structures and realized that the volume ratio V_A/V_B is largely determined by the three tilting angles. For an ideal cubic perovskite structure, $V_A/V_B = 5$. As octahedral tilting normally reduce the volume of NaF₁₂ polyhedra, distortion of the structure from the ideal cubic perovskite results in a decrease in the V_A/V_B ratio. The greater the distortion, the smaller the V_A/V_B ratio. Figure 8 shows the V_A/V_B ratio as a function of temperature at 4 GPa, indicating a decrease in the structure distortion when the sample temperature approaches the transition temperature. The V_A/V_B ratios calculated from ambient pressure data (Zhao et al.

1993a) are also plotted in Figure 8 for comparison. Lower V_A/V_B ratios at higher pressure indicate that the structure distortion becomes more significant at high pressure.

Based on a simple model of ionic overlaps, Magyari-Köpe et al. (2002) investigated over twenty orthorhombic perovskite samples and concluded that pressure drives the perovskite system toward a less distorted crystal structure. They predicted hardening of MgO₁₂ polyhedron relative to SiO₆ octahedron in MgSiO₃ perovskite at extremely high pressures and an orthorhombic-cubic transition when MgSiO₃ is compressed by 64% in volume, although they recognized that the structure distortion of MgSiO₃ perovskite may increase with compression. Our crystal chemical data at high pressure and temperature demonstrate that pressure drives the NaMgF₃ perovskite toward a more distorted crystal structure, inconsistent with the predictions of the general trend in the structure change with pressure in the orthorhombic perovskite system (Magyari-Köpe et al. 2002). As an isostructural and isoelectronic analogue of NaMgF₃, MgSiO₃ perovskite may exhibits persistence of the orthorhombic structure at high pressures. This is consistent with experimental observations and theoretical calculations (Kudoh et al. 1987; Mao et al. 1991; Stixrude and Cohen 1993; Funamori and Yagi 1993).

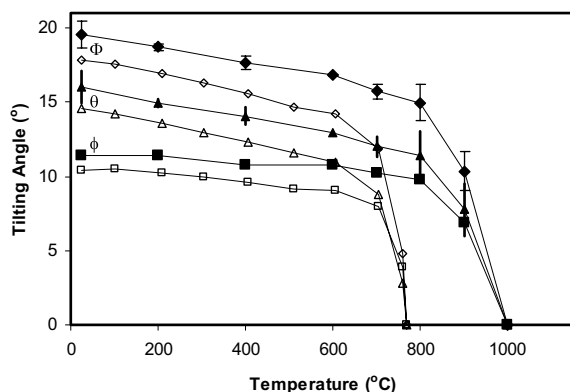


FIGURE 7. The octahedral tilting angle Φ , θ , and ϕ of the NaMgF₃ structure at 4 GPa (solid symbols) and ambient pressure (open symbols, after Zhao et al. 1993a). The bars attached to the symbols represent the experimental errors (some are smaller than the symbols).

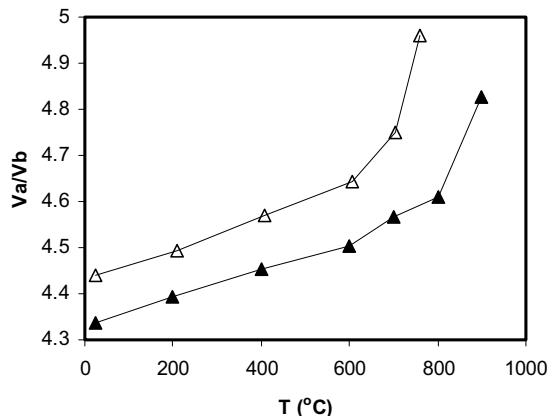


FIGURE 8. The V_A/V_B ratio of the NaMgF₃ structure at 4 GPa (solid symbols) and ambient pressure (open symbols, after Zhao et al. 1993a).

ACKNOWLEDGMENTS

The research was carried out (in part) at the National Synchrotron Light Source, Brookhaven National Laboratory, which is supported by the U.S. Department of Energy, Division of Materials Sciences and Division of Chemical Sciences, under contract no. DE-AC02-98CH10886. This research was partially supported by COMPRES, the Consortium for Materials Properties Research in Earth Sciences under NSF Cooperative Agreement EAR 01-35554. The study was also supported by NSF Research Grants (EAR0125094, EAR-0510501, and EAR9909413). We thank M. Vaughan, L. Wang, and Z. Zhong for their technical support at the X17 beamline. MPI pub. no. 355.

REFERENCES CITED

- Chakhmouradian, A.R., Ross, K., Mitchell, R.H., and Swainson, I. (2001) The crystal chemistry of synthetic potassium-bearing neightborite, (Na_{1-x}K_x)MgF₃. *Physics and Chemistry of Minerals*, 28, 277–284.
- Chao, E.C.T., Evans, H., Skinner, B., and Milton, C. (1961) Neighbourite, NaMgF₃, a new mineral from the Green River Formation, South Uray, Utah. *American Mineralogist*, 46, 379–393.
- Chen, J., Parise, J.B., Li, R., Weidner, D.J., and Vaughan, M. (1998a) The imaging plate system interfaced to the large-volume press at beamline X17B1 of the National Synchrotron Light Source. In M.H. Manghnani and T. Yagi, Eds., *Properties of Earth and Planetary Materials at High Pressure and Temperature*, Geophysical Monograph 101, p. 139–144. American Geophysical Union, Washington D.C.
- Chen, J., Weidner, D., Vaughan, M., Li, R., Parise, J., Koleda, C., and Baldwin, K. (1998b) Time resolved diffraction measurements with an imaging plate at high pressure and temperature. *Review of High Pressure Science and Technology*, 7, 272–274.
- Decker, D.L. (1971) High-pressure equation of state for NaCl, KCl and CsCl. *Journal of Applied Physics*, 42, 3239–3244.
- Egami, T. and Billinge, S.J.L. (2003) *Underneath the Bragg Peaks: Structural Analysis of Complex Materials*. Elsevier, Kidlington.
- Funamori, N. and Yagi, T. (1993) High pressure and high temperature in situ X-ray observation of MgSiO₃ perovskite under lower mantle conditions. *Geophysical Research Letters*, 20, 387–390.
- Glazer, A.M. (1972) The classification of tilted octahedra in perovskite. *Acta Crystallographica*, B 28, 3384–3392.
- Ito, E. and Yamada, H. (1982) Stability relations of silicate spinels, ilmenites, and perovskite. In S. Akimoto and M.H. Manghnani, Eds., *High Pressure Research in Geophysics*, p. 405–419. Center for Academic Publications Japan, Tokyo.
- Kudoh, Y., Ito, E., and Takeda, H. (1987) Effect of pressure on the crystal structure of perovskite-type MgSiO₃. *Physics and Chemistry of Minerals*, 14, 350–354.
- Larson, A.C. and Von Dreele, R.B. (1986) GSAS, General Structure Analysis System. Los Alamos National Laboratory, New Mexico.
- Ludkens, W.L.W. and Welch, A.J.E. (1952) Reactions between metal oxides and fluorides: some new double-fluoride structures of type ABF₃. *Acta Crystal-*

- lographica, 5, 841.
- Magyari-Köpe, B., Vitos, L., Johansson, B., and Kollár, J. (2002) Origin of octahedral tilting in orthorhombic perovskites. *Physical Review*, B 66, 092103 1–4.
- Mao, H.K., Hemley, R.J., Fei, Y., Shu, J.F., Chen, L.C., Jephcoat, A.P., Wu, Y., and Bassett, W.A. (1991) Effect of pressure, temperature, and composition on lattice parameters and density of (Fe,Mg)SiO₃-perovskites to 30 GPa. *Journal of Geophysical Research*, B, Solid Earth and Planets, 96, 8069–8079.
- Murakami, M., Hirose, K., Kawamura, K., Sata, N., and Ohishi, Y. (2004) Post-perovskite phase transition in MgSiO₃. *Science*, vol 304, Issue 5672, 855–858. [DOI: 10.1126/science.1095932].
- O'Keefe, M. and Bovin, J.-O. (1979) Solid electrolyte behavior of NaMgF₃: Geophysical implications. *Science*, 206, 599–600.
- O'Keefe, M. and Hyde, B.G. (1977) Some structures topologically related to cubic perovskite (E21), ReO₃ (D09) and Cu₂Au (L12). *Acta Crystallographica B*, 33, 3802–3813.
- O'Keefe, M., Hyde, B.G., and Bovin, J.-O. (1979) Contribution to the crystal chemistry of orthorhombic perovskite: MgSiO₃ and NaMgF₃. *Physics and Chemistry of Minerals*, 4, 299–305.
- Ringwood, A.E. (1962) Mineralogical constitution of the deep mantle. *Journal of Geophysical Research*, 67, 4005–4010.
- Rönnebro, E., Noréus, D., Kadir, K., Reiser, A., and Bogdanovic, B. (2000) Investigation of the perovskite related structures of NaMgH₃, NaMgF₃ and Na₂AlH₆. *Journal of Alloys and Compounds*, 299, 101–106.
- Saxena, S.K., Dubrovinsky, L.S., Lazor, P., Cerenius, Y., Haggkvist, P., Hanfland, M., and Hu, J. (1996) Stability of perovskite (MgSiO₃) in the Earth's mantle. *Science*, 274, 1357–1359.
- Saxena, S.X., Dubrovinsky, L.S., Lazor, P., and Hu, J. (1998) In situ-X-ray study of perovskite (MgSiO₃); phase transition and dissociation at mantle conditions. *European Journal of Mineralogy*, 10, 1275–1281.
- Shim, S.-H., Duffy, T.S., and Shen, G. (2001) Stability and structure of Mg-SiO₃ perovskite to 2300-kilometer depth in Earth's mantle. *Science*, 293, 2437–2440.
- Shim, S.-H., Jeanloz, R., and Duffy, T.S. (2002) Tetragonal structure of CaSiO₃ perovskite above 20 GPa. *Geophysical Research Letters*, 29(24), 2166, doi: 10.1029/2002GL016148.
- Stixrude, L. and Cohen, R.E. (1993) Stability of orthorhombic MgSiO₃ perovskite in the Earth's lower mantle. *Nature*, 364, 613–616.
- Street, J.N., Wood, I.G., Knight, K.S., and Price, G.D. (1997) The influence of thermal vibrations on the average structure of cubic NaMgF₃ perovskite: a combined molecular dynamics and neutron diffraction study. *Journal of Physics: Condensed Matter*, 9, L647–L655.
- Thomas, N.W. (1996) The compositional dependence of octahedral tilting in orthorhombic and tetragonal perovskites. *Acta Crystallographica*, B52, 16–31.
- — — (1998) A new global parameterization of perovskite structures. *Acta Crystallographica*, B54, 585–599.
- Wang, Y., Guyot, F., and Liebermann, R.C. (1992) Electron microscopy of (Mg,Fe)SiO₃ perovskite: Evidence for structural phase transitions and implications for the lower mantle. *Journal of Geophysical Research*, 97, 12,327–12,347.
- Weidner, D.J., Vaughan, M.T., Ko, J., Wang, Y., Leinenweber, K., Liu, X., Yeganeh-Haeri, A., Pacalo, R.E., and Zhao, Y. (1992) Large volume high pressure research using the wiggler port at NSLS. *High Pressure Research*, 8, 617–623.
- Zhao, Y., Weidner, D.J., Parise, J.B., and Cox, D.E. (1993a) Thermal expansion and structural distortion of perovskite—data for NaMgF₃ perovskite. Part I. *Physics of the Earth and Planetary Interiors*, 76, 1–16.
- — — (1993b) Thermal expansion and structural distortion of perovskite—data for NaMgF₃ perovskite. Part II. *Physics of the Earth and Planetary Interiors*, 76, 17–34.
- Zhao, Y., Parise, J.B., Wang, Y., Kusaba, K., Vaughan, M.T., Weidner, D.J., Kekegawa, T., Chen, J., and Shimomura, O. (1994a) High-pressure crystal chemistry of neighborite, NaMgF₃: An angle-dispersive diffraction study using monochromatic synchrotron X-radiation. *American Mineralogist*, 79, 615–621.
- Zhao, Y., Weidner, D.J., Ko, J., Leinenweber, K., Liu, X., Li, B., Meng, Y., Pacalo, R.E.G., Vaughan, M.T., Wang, Y., and Yeganeh-Haeri, A. (1994b) Perovskite at high P-T conditions: An *in-situ* synchrotron X-ray diffraction study of NaMgF₃ perovskite. *Journal of Geophysical Research*, 99, 2871–2885.
- Zhou, L.X., Hardy, J.R., and Cao, H.Z. (1997) Molecular dynamics simulation of superionicity in neighborite, NaMgF₃. *Geophysical Research Letters*, 24, 747–750.

MANUSCRIPT RECEIVED MAY 11, 2004

MANUSCRIPT ACCEPTED FEBRUARY 11, 2005

MANUSCRIPT HANDLED BY SANG-HEON DAN SHIM